Chemical Abundances of CH Stars in Omega Centauri

A Senior Honors Thesis

Presented in Partial Fulfillment of the Requirements for Graduation with Distinction in Astronomy in the Undergraduate College of Arts and Sciences of The Ohio State University

By

Elizabeth M. Otto

The Ohio State University

May 2012

Project Adviser: Professor Jennifer Johnson

ABSTRACT

Omega Centauri (hereafter ω Cen), the largest globular cluster in the Galaxy, is an important environment for studying nucleosynthesis because of its significant abundance variations and evidence of multiple stellar generations. The cluster also contains several known CH stars, which are thought to be the result of past binary mass transfer from an asymptotic giant branch (AGB) companion. CH stars are thus hypothesized to be a good probe of AGB nucleosynthesis. We use the CH stars in ω Cen to test this assumption. We compare the elemental abundances of CH stars within the cluster to those of CH stars outside the cluster to test the effects of the formation environment on the abundances of AGB nucleosynthesis products. We also compare the chemical abundances of the ω Cen CH stars to other red giants in the cluster to determine if the same processes are responsible for the chemical enrichment of both the CH stars and the cluster. In general, we find that the CH stars in ω Cen have similar abundances to CH stars in the field. We also find that as metallicity increases, the s-process abundances of stars in ω Cen approach those of the CH stars, indicating that similar mechanism is responsible for the enrichment in both cases.

1. INTRODUCTION

1.1. Stellar Nucleosynthesis

Stars produce most of the chemical elements in the universe through various paths of nucleosynthesis. There are two main processes that produce nuclei heavier than iron, known as the r-process and the s-process respectively. The r-process signifies the *rapid* neutron capture process, while the s-process signifies the *slow* neutron capture process. The speed of these processes refers to the speed of the neutron capture with respect to the timescale of β (beta) decay. Beta decay operates by transforming a neutron into a proton and other particles:

$$n \rightarrow p + e^{-} + \bar{\nu_e} \tag{1}$$

This process results in an element with the same mass number, but a higher atomic number:

$${}^{A}_{Z}N \rightarrow {}^{A}_{Z+1}N' + e^{-} + \bar{\nu_e} \tag{2}$$

Since the r-process adds neutrons quickly compared to the rate of β decay, nuclei become quite heavy, and then decay down to the valley of stability after the neutron flux has dropped.

By contrast, the s-process can only create nuclei in the valley of stability, since β decay occurs quickly compared to the addition of neutrons. This means that the s-process and r-process produce different isotopes and elements. We can therefore use specific elements to probe each process. For instance, theory suggests that most barium is produced in the s-process, while most europium is produced in the r-process (Arlandini et al. 1999).

The sites where these processes can potentially occur are limited by the neutron flux necessary for a particular process. The r-process is hypothesized to operate primarily in core-collapse supernovae (Meyer 1994, e.g.). These explosions, which occur when a massive star runs out of fuel, also distribute iron peak elements. This proposal is supported by the fact that the r-process appears to dominate the s-process at early times in the Galaxy, since chemical abundances in old stars are consistent with the solar r-process pattern (Truran 1981; Sneden & Parthasarathy 1983; Sneden & Pilachowski 1985). The timescale of enrichment with both iron and r-process elements in early generations of stars suggests that the r-process must have operated in the first stellar generation, which suggests a source stemming from short-lived, massive stars (Meyer 1994).

By contrast, the s-process is hypothesized to operate primarily in thermally pulsing asymptotic giant branch (TP-AGB) stars. Asymptotic giant branch, or AGB, stars have exhausted the helium in their core by burning it to carbon, and nuclear fusion occurs in shells around the inert core. On the TP-AGB, the energy production is normally dominated by the H shell, but the He shell undergoes thermonuclear runaway flash events that start complicated mixing and convective processes (Herwig 2005). This process drives third dredge-up, which brings some protons into regions mostly composed of He and C. In turn, this is hypothesized to drive the formation of a ^{13}C pocket, where nuclear fusion reactions produce neutrons:

$$^{13}_{6}C +^{4}_{2} He \rightarrow^{16}_{8} O + n \tag{3}$$

This process produces a low neutron density, but operates on a relatively large timescale (Cristallo et al. 2011).

Based on observations of the chemical makeup of the Sun and other nearby stars, there are three main peaks in the distribution of s-process elements. These peaks occur near mass numbers of 87, 138, and 208 (Meyer 1994). The process described above drives the so-called main component of the s-process, which corresponds to the peak at mass number 138 and produces elements like barium and lanthanum. These elements are generally referred to as high mass s-process elements, or *hs* elements. A second neutron source is generally needed to reproduce the low mass peak, which corresponds to elements like yttrium and zirconium. Some theories suggest that this additional neutron source may stem from the burning of neon, but results are inconclusive for low mass stars (Cristallo et al. 2011). These are the

low mass s-process elements, or *ls* elements. This process may operate in different types of stars or at different times in the evolution than the main component of the s-process.

1.2. CH Stars

CH stars are carbon-enhanced, metal-poor stars that have significant CH molecular bands in their spectra. They are identified on the basis of these molecular bands, but they have other unique characteristics. Typically, they also show enhanced abundances of s-process elements such as barium (Ba) and lanthanum (La) (Vanture 1993). They are not yet on the AGB, and thus could not have produced their chemical irregularities through their own nucleosynthesis. These objects are also metal-poor and are likely a low metallicity counterpart to Ba stars. Currently, these stars are hypothesized to form in a binary mass transfer episode. At some point in its history, the CH star had a companion that evolved onto the AGB, where it became extremely large and produced a strong wind. This wind deposited material rich in the products of AGB nucleosynthesis onto the star, producing significantly enhanced carbon (C) and s-process abundances. The AGB star likely eventually evolved into a white dwarf, and essentially faded from sight. The CH star then evolved onto the RGB, becoming significantly brighter in the process. Today, the CH star is visible with unusual spectral features and chemical composition.

This theory on CH star formation originated when it was discovered that the majority of both Ba and CH stars are in binary systems (McClure 1984). The scenario suggests that CH stars may preserve a record of AGB nucleosynthesis products. Since the s-process in particular is still poorly understood, this record is potentially important for the study of how the heavy elements are formed. However, the hypothesis that CH stars act as a pure chemical record of AGB nucleosynthesis has as yet not been tested. For instance, since initial chemical abundances of stars are often strongly correlated to the formation environment, the effects of the transferred material may be dependent upon or subsumed by the chemical character of the surrounding environment. If the amount of transferred material is not enough to swamp the unique chemical signature of the formation environment, then CH stars would make a poor probe of AGB nucleosynthesis.

Alternatively, the chemical abundances may be strongly dependent on the amount of transferred material or when this material is transferred. In turn, these properties may be dependent on the closeness of the binary system. For instance, if the envelope of an AGB star is stripped completely before dredge-up can occur, then the ^{13}C pocket necessary for s-process nucleosynthesis may never form. Cristallo et al. (2011) and Stancliffe & Jeffery (2007) both consider the effects of mass loss on the nucleosynthetic yields of low-mass AGB

stars. Stancliffe & Jeffery (2007) find that while the mass loss law leads to negligible differences in the yields of most isotopes, differences can occasionally approach a factor of ten. Furthermore, Cristallo et al. (2011) find that the variations in mixing based on how much of the envelope has been stripped lead to both lower absolute surface abundances and a change in the shape of the s-process distribution (in the form of a changing $[hs/ls]$ ratio). These effects could operate to change the abundance of transferred material relative to the s-process that operates in non-binary AGB stars. In summary, there are several effects that could potentially make CH stars less useful as a window into AGB nucleosynthesis processes.

1.3. ω Cen

Globular clusters are some of the most studied astronomical objects in the Galaxy. They are large, dense, spherical groups of stars. These stars often formed and evolved at the same time, and so provide astronomers with an environment in which to test theories of stellar evolution (Gratton et al. 2004). ω Cen is the largest such cluster in the Milky Way, with a mass of over $5 \times 10^6\, M_\odot$ (Meylan et al. 1995). However, it shows significant evidence for multiple stellar generations, indicating that it is not a simple system of stars that evolved more or less simultaneously. This evidence includes the formation of multiple main sequences and red giant branches in color-magnitude diagrams. An example of this evidence is shown in Figure 1. Stars within ω Cen show strong chemical abundance variations as a function of metallicity, which provides further proof of multiple generations of stars. While other globular clusters have variations in some chemical abundances, ω Cen is one of the only objects that shows substantial variations in iron abundances, indicating that it was enriched over its lifetime not just by AGB nucleosynthesis products, but also by the products of Type II supernovae.

Theories on the origin of ω Cen are varied. Current evidence suggests that it is likely the remaining core of a tidally disrupted dwarf galaxy that collided with the Milky Way (Dinescu et al. 1999). This scenario explains the chemical enrichment and stellar generations in the cluster, since Galactic globular clusters more typically have only a single star formation episode. It also provides a mechanism for the formation of the blue main sequence in ω Cen , which appears to be helium rich (Bekki & Norris 2006). Other theories, including the merger of two globular clusters native to the Milky Way, are unable to reproduce the kinematics of the system (Dinescu et al. 1999). The recent chemical evolution of ω Cen is dominated by the products of AGB nucleosythesis (Smith et al. 2000). However ω Cen formed, its nature as a dense environment with identifiable trends in chemical abundances as a function of metallicity make it an ideal place to study the effects of formation environment

on stellar objects.

1.4. Motivation

We set out to test the assumption that CH stars are a good probe of the s-process. For this test, the CH stars found in ω Cen can be used. The location of these stars gives the analysis several advantages. First, as mentioned above, ω Cen has distinct patterns in chemical abundance as a function of metallicity. If in ω Cen CH stars show the same trends with metallicity as cluster members in s-process abundances, then the assumption of AGB mass transfer overwhelming the initial abundances is incorrect. This would mean that CH stars would not be a probe of AGB nucleosynthesis processes. Second, the relative s-process abundances of CH stars inside and outside ω Cen can be compared. If the chemical abundances are similar, then this would indicate that the impact of formation environment or the closeness of the binary system is minimal, and that CH star abundances are potentially reflective of AGB nucleosynthesis. Finally, as mentioned above, ω Cen's heavy element chemical evolution is dominated by the products of the s-process. Since the same process is enriching both the CH stars (in a single episode) and the cluster (over the course of time), the s-process abundances of cluster giants to those of the CH stars can be compared. If they converge as metallicity increases in the cluster, then this indicates that the two sets of chemical abundances are reflective of the same process. In turn, this would demonstrate that CH star abundances are reflective of the s-process. Over the course of this analysis, we make these three major comparisons to test the hypothesis that CH stars are a probe of AGB nucleosynthesis.

This thesis is organized as follows: in §2 I briefly review the observations and our data reduction procedures. In §3 I describe the techniques for measuring stellar parameters and chemical abundances. In §4 the chemical abundance data is presented and analyzed. Finally, in §5 the conclusions of the analysis are summarized.

2. OBSERVATIONS

2.1. Sample Selection and Observations

The sample of ω Cen red giants was taken from the Royal Observatory Annals (ROA) 1966 catalogue, which includes over 600 objects in the cluster (Royal Greenwich and Cape Observatories 1966). The final sample encompasses 57 red giants in the cluster and includes two CH stars - ROA 55 and ROA 70. Stars in the catalogue are quite bright, and our

sample has V magnitudes ranging from 11.2 mag to 13.1 mag. Additional calibration data of abundance standards (such as HD 122563) were also obtained. High resolution spectra were obtained with the Echelle Spectrograph on the 2.5 meter DuPont Telescope at Las Campanas Observatory. Observations were taken in March 2000, June 2000, and May 2001. The spectra have a typical resolution of R=40,000, and span a wavelength range from 3500 Å to 8000 Å. Information on these objects, including ROA and LEID (van Leeuwen et al. 2000) identifiers as well as coordinates and date of observation are listed in Table 1. Coordinates are obtained either from van Leeuwen et al. (2000) or Royal Greenwich and Cape Observatories (1966). For objects not covered in the van Leeuwen survey, V magnitudes were taken from the ROA catalogue, which is significantly less accurate. Because of time limitations, we have only analyzed 14 of the objects. This includes both of the CH stars. The stars analyzed were chosen because their spectra have high signal-to-noise and they span a wide range in metallicity.

2.2. Data Reduction

The data were corrected using an overscan region, and then trimmed and biased using standard procedures in IRAF. Because of the complicated nature of the echelle spectrograph and the detector, flat fields are difficult to construct. The correction was initially made using 'milky flats,' which attempt to diffuse light over the detector in a way that mimics the observations. These were combined, then boxcar smoothed to create flat field. However, their application did not significantly or systematically change derived equivalent widths. Furthermore, milky flats were not available for all months of observation. For these reasons, most of our fully reduced data was not flat-fielded.

This spectrograph produces significant scattered light in red wavelengths. This effect must be taken into account - without a scattered light correction, equivalent widths will be systematically underestimated. This introduces wavelength-dependent trends in abundances. The IRAF task *apscatter* was used to create a 2D model of the scattered light. Once the scattered light solution was applied, spectra were extracted using fits to the echelle orders determined using observed bright giants from the same night. However, the scattered light model is not completely accurate, and this makes measurement of spectral lines at wavelengths greater than 6500 $\mathring{A}$ suspect.

The wavelength calibration was determined using exposures of a ThAr (thorium-argon) lamp. Spectra of this lamp were then correlated with an atlas of ThAr spectral lines. Lines were initially identified by eye. Once the basic wavelength solution was in place, iterative automated coordinate matching allowed for the identification of roughly 1000 spectral lines.

The order of the wavelength solution was then adjusted to remove any trends with line or column on the chip. Independent wavelength solutions were found for each month of observation; however, the instrument is sufficiently stable over shorter periods of time that further solutions were not necessary. All identification and fitting related to the wavelength solution was performed using the IRAF task *ecidentify*. The r.m.s. for the wavelength calibration fit was approximately $0.01\,\mathring{A}$. The wavelength solution was then applied to the data.

For a spectrum to be ready for analysis, the spectrum of the star was shifted to the rest frame. The radial velocity was measured using the IRAF task *rvidlines*. Generally, the most identifiable lines came from the Fe-I linelist. The radial velocity was measured from roughly ten lines across several orders and then averaged. The spectrum was then shifted so that the rest wavelengths of spectral lines matched the wavelength solution. Finally, the blaze was fit by eye in SPECTRE and removed to make equivalent width measurement possible. A fully reduced sample spectrum from one echelle order, with the blaze removed, is shown in Figure 2.

3. ANALYSIS

3.1. Determining Stellar Parameters

To determine chemical abundances, a model stellar atmosphere must be constructed. For the stellar model to be accurate, four parameters must first be specified. The first is effective temperature, or T_{eff}, which is related to the surface temperature of the star. The temperature of the star dictates the number of electrons in any energy level of an atom, and thus partially determines the strength of a given spectral feature. This effect is quantified by the Boltzmann equation:

$$\frac{N_b}{N_a} = \frac{g_b}{g_a} e^{-(E_b - E_a)/kT} \tag{4}$$

In this equation, a and b are two energy states for the electron. E_a and E_b are the energies associated with these states, and g_a and g_b are the degeneracies of these states. N_a and N_b are the number of atoms with electrons in the given states a and b. To first order, the temperature dictates the strength of any given spectral feature because it determines the relative population of energy states. The effective temperature, or T_{eff} is defined to be the temperature of a blackbody of the same bolometric luminosity as the star in question. This means that:

$$L_{bol} = 4\pi R^2 \sigma T_{eff}^4 \tag{5}$$

Both the bolometric luminosity and the radius of a star are difficult to measure. Instead, astronomers use the color of a star, which is based on the difference between photometric measurements in different bands. Alternatively, the effective temperature can be determined spectroscopically.

The second parameter is $log(g)$, which probes the surface gravity of the star and is generally measured in cgs units. The surface gravity of any spherical object is given by:

$$g = \frac{GM}{R^2} \tag{6}$$

where M is the mass and R is the radius of the object. As surface gravity increases, the pressure and density of gas in the star at any given radius from the center of the star increases. According to the Saha equation, the ionized fraction of any given species, X, is dependent on both the temperature and the density:

$$\frac{X}{1-X^2} = \frac{1}{nh^3}(2\pi m_e kT)^{3/2} e^{-I/kT} \tag{7}$$

Here, n is the density, m_e is the electron mass, T is the temperature, and I is the ionization energy. Therefore, the surface gravity of the star influences the relative amount of any given element that is ionized.

The third parameter is the metallicity, or [Fe/H], which can be determined using the equivalent widths of the Fe-I (neutral) and Fe-II (singly ionized) lines. Iron is used as a proxy for the metal content of the star, where metals are defined to be all elements heavier than He. Finally, the microturbulent velocity, or v_t, characterizes the relative spread in line-of-sight speeds of gas on the surface of the star. The speed of the gas relative to the overall velocity of the star produces a Doppler effect, where some light from a particular spectral feature will be shifted slightly to the blue, and other light slightly to the red. The relative spread in the speed of the gas determines the extend this effect will broaden the spectral feature.

To determine these parameters, the equivalent widths of Fe-I and Fe-II lines are measured. Since the objects in our sample are generally well studied, we use estimates of the parameters from other sources (Stanford et al. 2006; Johnson & Pilachowski 2010) as a starting point for creating atmosphere models. We use the MARCS stellar model atmosphere grid and interpolation to create spherical LTE model atmospheres with the correct parameters (Gustafsson et al. 2008). The spectral synthesis tool MOOG is used to derive the abundances of Fe-I and Fe-II based on the model atmosphere and measured equivalent widths. To determine parameters, we impose the following conditions:

1. There should be no trend in derived abundances of Fe-I with the excitation potential. This requirement helps determine T_{eff}.

2. The iron abundances derived from Fe-I and Fe-II lines should be equal. This requirement helps determine $log(g)$.

3. There should be no trend in abundance as a function of reduced equivalent width (defined as the equivalent width divided by the wavelength). This requirement determines v_t.

We iterate over model parameters until these conditions are achieved. The final parameters determine the metallicity, where the model and derived metallicity should be approximately the same. Determination of stellar parameters is more difficult for cooler stars, where the models are less reliable and equivalent widths are more difficult to measure.

Since the parameters are often difficult to determine for cooler stars, we also use photometric temperatures and physical gravities, which provide an alternative way of measuring parameters independent of the spectrum. The $(V - K_s)$ color is derived from the values presented in Table 1. The effective temperature is then calculated according to Ramírez & Meléndez (2005) with:

$$T_{eff} = \frac{5040\,K}{\theta_{eff}} \tag{8}$$

$$\theta_{eff} = 0.4405 + 0.3272(V - K_s) - 0.0252(V - K_s)^2 \tag{9}$$

A measure of the surface gravity in terms of bolometric magnitude can be derived from equations 4 and 5. This physical gravity is given by Kraft & Ivans (2003) as:

$$log_{10}(\frac{g}{g_\odot}) = log_{10}(\frac{M}{M_\odot}) - 4log_{10}(\frac{5770\,K}{T_{eff}}) - 0.4(4.72 - M_{bol}) \tag{10}$$

We adopt a stellar mass of $1.0\,M_\odot$. This mass is appropriate considering ω Cen's age and the fact that studied stars are on the red giant branch. The bolometric magnitude M_{bol} is given by:

$$M_{bol} = V + BC_V - 5log_{10}d + 5 - A_V \tag{11}$$

where V is the V band magnitude, BC_V is a bolometric correction for the V band, d is the distance to ω Cen, and A_V is the extinction in the V band towards ω Cen. We use the V band distance modulus to ω Cen from van de Ven et al. (2006), which gives $(m - M)_V = 3.75 \pm 0.13mag$. This value includes the extinction. We adopt the bolometric correction from Alonso et al. (1999):

$$X = log_{10}(T_{eff}) - 3.52 \tag{12}$$

$$BC_V = \frac{-0.05531}{X} - 0.6177 + 4.420X - 2.699X^2 \tag{13}$$

3.2. Measuring Chemical Abundances

Once the stellar parameters have been determined, other chemical abundances can be measured. I created lists of spectral lines and associated excitation potentials and transition probabilities for 20 elements: oxygen (O), sodium (Na), silicon (Si), calcium (Ca), scandium (Sc), titanium (Ti), vanadium (V), chromium (Cr), manganese (Mn), iron (Fe), cobalt (Co), nickel (Ni), yttrium (Y), zirconium (Zr), barium (Ba), lanthanum (La), praseodymium (Pr), neodymium (Nd), samarium (Sm), and europium (Eu). This sample encompasses α elements, iron peak elements, and common s-process and r-process elements. For most of these elements, I measured the equivalent widths using SPECTRE, and then used these measurements and model atmosphere to automatically determine the abundance using MOOG.

For elements with non-integer nuclear spins, it is necessary to take hyperfine splitting of spectral lines into account in order to avoid overestimating equivalent widths and abundances. The elements for which this is necessary include Sc, V, Mn, La, and Eu. Additionally, different isotopes of the same element have slightly different energy levels, producing splitting in spectral lines. This phenomenon is known as isotope shift, and is most relevant for Ba. To determine the abundances of these elements, we use the spectrum synthesis (*synth*) driver in MOOG, which allows the user to use an input line list and model to reproduce a given part of the spectrum. The input linelist was generated using the Kurucz molecular and atomic databases, which are available online at http://kurucz.harvard.edu. The abundance is then varied and changed by eye to produce the best fit to the spectral feature. A sample synthesis of a Ba-II line is shown in Figure 2.

3.3. Testing the Analysis

To determine if the data reduction and analysis were producing reasonable results, we compared the our measured equivalent widths for an abundance standard, HD122563, to equivalent widths published in Cayrel et al. (2004) and Johnson (2002). The results of this analysis are shown in Figure 3. There is a significant tendency to underestimate the equivalent widths without the application of the scattered light correction. Although there is still some scatter around the literature values with the scattered light subtraction applied, the overall mean deviation in equivalent width is $0.53\,m\mathring{A}$, with a standard deviation of $3.4\,m\mathring{A}$.

We also find that our derived metallicities are systematically lower than previously published values by, on average, $0.2\,dex$. We compare our metallicities to those derived by Johnson & Pilachowski (2010) and Pancino et al. (2011). In order to determine the root

of this difference, we tested our analysis in several ways. First, we used reduced spectra without the scattered light subtraction to determine if this was leading to a systematic underestimation in Fe-I equivalent widths. However, this change did not produce significant variation in the derived metallicity in the abundance standard HD122563 or in ROA 159. We also tested the effects of using ATLAS9 model atmospheres (Castelli et al. 1997) but did not find any systematic change in the output metallicity.

3.4. Error Analysis

To quantify the errors in our abundance measurements, we use a method that propagates the errors in the parameters to the chemical abundances. This requires first determining the uncertainties in the parameters. Our basic method is described in more detail in Epstein et al. (2010), but a brief summary is given here.

We identify four observables that relate to the parameters. These are:

1. o_1: Photometric temperature, based on $V - K_s$ color.
2. o_2: The slope the Ca-I abundance versus the reduced equivalent width ($log(EW/\lambda)$)
3. o_3: The physical gravity, which is based on a mass estimate, the T_{eff} estimate, and bolometric magnitude M_{bol}
4. o_4: The difference in metallicity for the model atmosphere and the output, which is given by [Fe I/H]$_{model}$-[Fe I/H]$_{output}$

We then write these observables as a linear combination of deviations from the selected model atmosphere. This is done by writing each observable as:

$$o_i = o_i^0 + \sum_{j=1}^{4} \frac{\partial o_i}{\partial m_j}(m_j - m_j^0) \tag{14}$$

where o_i^0 is the best-fit model value of an observable, and m_j represent varied model parameters. The model parameters are $m_1 = T_{eff}$, $m_2 = v_t$, $m_3 = log(g)$ and $m_4 = [Fe/H]$. We vary one model parameter at a time, with $\Delta m_1 = \pm 100\,K$, $\Delta m_2 = \pm 0.3 km\,s^{-1}$, $\Delta m_3 = \pm 0.3\,dex$, and $\Delta m_4 = \pm 0.2\,dex$. We then fit a linear trend to the varied models, so that we have a single value for the partial derivative for each pair of i and j. This forms a matrix of partial derivatives, which can be inverted to determine the errors in the parameters. The uncertainties in the parameters are listed in Table 2.

In this case, the observables o_1 and o_3 differ from those prescribed in Epstein et al. (2010). Because the model atmosphere parameters are related in complicated ways to the values of the observables, we choose to simplify the matrix by redefining o_1 as a photometric temperature and o_3 as physical gravity. These values are not dependent on model parameters outside T_{eff} and $log(g)$ respectively. The errors in these parameters can be determined using error propagation. In general, the spectroscopic and photometric values for T_{eff} generally agree to within $\pm 100\,K$. The physical and spectroscopic gravity values agree to, on average, $\pm 0.3\,dex$.

The uncertainties in the parameters can then be used to find the uncertainties in the abundances of all studied elements. Due to time limitations, it was not possible to complete the full error analysis for every star studied, so more work on error propagation is a key part of future work on this project. In general, we generated characteristic uncertainties in the abundances by varying the model parameters by Δm_1 and Δm_2 and averaging the changes in abundances.

4. RESULTS

4.1. Abundances of Light Elements

Abundances of the measured light elements for stars in the ω Cen sample, which include most α elements considered, are listed in Table 3. The abundances of these elements as a function of metallicity within ω Cen are plotted in Figures 4 and 5. Note that it was not possible to measure the abundances of every element for every star. O, Si, and Sc in particular have few or weak spectral features in the wavelength range of our analysis. Some features can be partially or totally swallowed by molecular bands.

In general, we reproduce the abundances of light elements as a function of metallicity in ω Cen found by other authors (Johnson & Pilachowski 2010; Smith et al. 2000). We find, on average, a mild (on order of 0.4 dex) enhancement in [O/Fe], with some decline as metallicity increases. While the highest metallicity stars have substantially higher [Na/Fe] values, the overall trend is difficult to distinguish because there are relatively few high metallicity stars in the sample. We find no substantial trends in [Ca/Fe] or [Sc/Fe]. We also find that [Ti/Fe] increases as metallicity increases. In general, CH star abundances of the light elements are consistent with the abundances of cluster giants.

4.2. Abundances of Iron Peak Elements

Abundances of the iron peak elements for stars in the ω Cen sample are listed in Table 4. These abundances as a function of [Fe/H] are plotted in Figures 5 and 6. Again, we find mostly the same trends in iron peak abundances as previous work. One exception is vanadium, which Smith et al. (2000) found to be slightly enhanced relative to iron. We find that, on average, [V/Fe] is generally less than zero. This difference may be due to the inclusion of hyperfine splitting in V-I spectral lines in this analysis.

In most elements, CH star abundances appear to be consistent with the abundances of the rest of the cluster. However, we do see anomalously high nickel abundances in the CH stars. There are few likely physical mechanisms to explain enhancement in Ni in products of AGB binary mass transfer. It is possible that Fe seed nuclei capture only a few neutrons, forming excess Ni, but this effect is not usually observed. It is also possible that the Ni lines may be blended with a molecular band in the CH stars, and finding correct abundances may require spectrum synthesis.

4.3. Abundances of Neutron Capture Elements

Since CH stars are hypothesized to be probes of AGB nucleosynthesis, it is most important to examine neutron capture elements, and particularly s-process elements. Abundances of the neutron capture elements, which encompass both low and high mass s-process elements, for the ω Cen sample are listed in Table 5. The abundances as a function of [Fe/H] for both CH stars and cluster giants are shown in Figures 7 and 8.

In general, we reproduce the trends in s-process and r-process abundances as a function of metallicity found in other work. We find enhancements of roughly 2 dex in Ba and La as metallicity increases in the cluster. We also find that the abundance of Eu as a function of [Fe/H] is relatively constant, which is consistent with both previous works. In general, the abundances of Y and Zr also increase as expected, since these are also s-process elements. However, there is considerably more scatter around the general increase as a function of metallicity in these elements as compared to Ba and La. This is likely due to a few effects. First, measurement of Y and Zr abundances is more difficult than measurement of Ba and La abundances. In particular, Zr lines are difficult to find and measure accurately. By contrast, Ba has several strong lines in the wavelength region we are studying. Secondly, Y and Zr are low mass s-process elements, and likely form in different environments than do Ba and La.

The s-process abundances of the CH stars in ω Cen are significantly enhanced compared

to cluster giants at a similar metallicity, as expected. Additionally, the two stars generally have similar abundances to each other. The neutron capture abundances of the two CH stars are the same to within the uncertainty on the measurements for all elements except Sm. Finally, we find that the [Eu/Fe] abundances of the CH stars show no difference from the rest of ω Cen, which is expected if they are the product of mass transfer from an AGB star.

5. DISCUSSION and CONCLUSIONS

It is evident from the abundances of Y, Zr, Ba, and La that the two studied CH stars have quite similar abundances of s-process elements despite a substantial difference in metallicity. The higher metallicity CH star (ROA 70) generally has slightly lower s-process abundances when compared to its lower metallicity counterpart (ROA 55). However, these differences are not significant compared to the uncertainties on the measurement. This comparison is a first test of the effect of formation environment on CH star abundances. Since the two CH stars have similar abundances, it appears that the effect of the transferred material is substantial enough to largely swamp any of the chemical abundance trends in ω Cen as a whole.

We can compare the abundances of the CH stars in ω Cen and cluster giants to the s-process and r-process yields, as well as to the solar abundance pattern. This comparison is shown for ROA 55 (a CH star) and ROA 159 (a giant in ω Cen) in Figure 9. The solar chemical abundances are taken from Grevesse & Sauval (1998), while the r-process and s-process predictions are calculated from Arlandini et al. (1999). All values are scaled to the metallicity of the star in question. Note that while ROA 159 generally follows the scaled solar pattern, ROA 55 shows significant enhancements in the products of s-process nucleosynthesis. While the abundance pattern of ROA 55 most closely follows an enhanced s-process prediction, the samarium abundance is anomalously high.

In order to help discern the effects of formation environment on the chemical abundances of CH stars, we compare them to abundances for field CH stars, from a variety of sources (Vanture 1992; Goswami & Aoki 2010; Pereira & Junqueira 2003; Johnson & Bolte 2004). In this case, we use the [Eu/La] ratio as a probe of the relative importance of the r and s processes. If CH stars are potential probes of AGB nucleosynthesis processes, the chemical signal from the transferred material must swamp the effects of the formation environment. Since the transferred material is rich in the products of the s-process, we would expect that CH stars would have a uniformly low [Eu/La] ratio regardless of metallicity or formation environment.

The results of this analysis are plotted in Figure 10. While not every CH star has exactly the same [Eu/La] ratio, they do fall in a defined region of the graph. In general, CH stars have an [Eu/La] ratio of near -0.75, with no discernible trend as function of metallicity. Furthermore, the CH stars from ω Cen have similar [Eu/La] ratios to CH stars outside globular clusters. This similarity indicates that there are no substantial effects changing the chemical enhancement caused by the binary mass transfer process in ω Cen. The relative similarity in r-process to s-process ratios for CH stars regardless of location indicates that the closeness of the binary, at least for this sample, likely has little effect on the chemical abundances of the transferred material.

The cluster giants in ω Cen are also included in Figure 10. Since the chemical evolution of ω Cen is dominated by the s-process, higher metallicity stars have substantially higher [La/Fe] values (see Figure 7) than do low metallicity cluster members. In some ways the cluster and the CH stars are being enriched by the same process: the CH stars get s-process products in a single event, while the rest of ω Cen is gradually enriched with the products of s-process nucleosynthesis over time. This means that higher metallicity ω Cen giants should have similar [Eu/La] values to CH stars. This hypothesis is borne out - higher metallicity giants in ω Cen have similar [Eu/La] ratios to the CH stars both inside and outside ω Cen . This similarity helps reinforce the idea that there is little difference between the s-process occurring in binaries and the s-process occurring in single AGB stars.

In summary, the CH stars in ω Cen have the expected strong enhancements in the products of s-process nucleosynthesis. They have similar abundances to CH stars outside globular clusters, indicating that formation environment is not substantially impacting the chemical abundances of the transferred material. The higher metallicity giants in ω Cen show similar neutron capture element abundances to the CH stars, indicating that the same s-process is responsible for the enrichment in both cases.

6. ACKNOWLEDGEMENTS

Many thanks to my adviser, Dr. Jennifer Johnson, for her extensive help and dedication to the project. In addition, Courtney Epstein provided substantial help with abundance analysis and error propagation questions. Much of this research was completed as a part of the Department of Astronomy Summer Undergraduate Research Program (SURP).

REFERENCES

Alonso, A., Arribas, S., & Martínez-Roger, C. 1999, A&AS, 140, 261

Arlandini, C., Käppeler, F., Wisshak, K., et al. 1999, ApJ, 525, 886

Bartkevicius, A. 1996, Baltic Astronomy, 5, 217

Bedin, L. R., Piotto, G., Anderson, J., et al. 2004, ApJ, 605, L125

Bekki, K., & Norris, J. E. 2006, ApJ, 637, L109

Busso, M., Gallino, R., & Wasserburg, G. J. 1999, ARA&A, 37, 239

Castelli, F., Gratton, R. G., & Kurucz, R. L. 1997, A&A, 318, 841

Cayrel, R., Depagne, E., Spite, M., et al. 2004, A&A, 416, 1117

Churchill, C. W., & Allen, S. L. 1995, PASP, 107, 193

Cote, P., Hanes, D. A., McLaughlin, D. E., et al. 1997, ApJ, 476, L15

Cowley, A. P., & Crampton, D. 1985, PASP, 97, 835

Cristallo, S., Piersanti, L., Straniero, O., et al. 2011, ApJS, 197, 17

Dinescu, D. I., Girard, T. M., & van Altena, W. F. 1999, AJ, 117, 1792

Epstein, C. R., Johnson, J. A., Dong, S., et al. 2010, ApJ, 709, 447

Freeman, K. C., & Rodgers, A. W. 1975, ApJ, 201, L71

Goswami, A., & Aoki, W. 2010, MNRAS, 404, 253

Gratton, R. G. 1982, A&A, 115, 336

Gratton, R., Sneden, C., & Carretta, E. 2004, ARA&A, 42, 385

Grevesse, N., & Sauval, A. J. 1998, Space Sci. Rev., 85, 161

Gustafsson, B., Edvardsson, B., Eriksson, K., et al. 2008, A&A, 486, 951

Han, Z., Eggleton, P. P., Podsiadlowski, P., & Tout, C. A. 1995, MNRAS, 277, 1443

Herwig, F. 2005, ARA&A, 43, 435

Ivans, I. I., Kraft, R. P., Sneden, C., et al. 2001, AJ, 122, 1438

Johnson, C. I., & Pilachowski, C. A. 2010, ApJ, 722, 1373

Johnson, J. A., & Bolte, M. 2004, ApJ, 605, 462

Johnson, J. A. 2002, ApJS, 139, 219

Kraft, R. P., & Ivans, I. I. 2003, PASP, 115, 143

Lai, D. K., Bolte, M., Johnson, J. A., et al. 2008, ApJ, 681, 1524

Lee, Y.-W., Joo, S.-J., Han, S.-I., et al. 2005, ApJ, 621, L57

Lloyd Evans, T. 1986, South African Astronomical Observatory Circular, 10, 1

McClure, R. D. 1997, PASP, 109, 536

McClure, R. D. 1984, ApJ, 280, L31

Meyer, B. S. 1994, ARA&A, 32, 153

Meylan, G., Mayor, M., Duquennoy, A., & Dubath, P. 1995, A&A, 303, 761

Norris, J. 1974, ApJ, 194, 109

Norris, J. E. 2004, ApJ, 612, L25

Norris, J. E., & Da Costa, G. S. 1995, ApJ, 447, 680

Paltoglou, G., & Norris, J. E. 1989, ApJ, 336, 185

Pancino, E., Mucciarelli, A., Sbordone, L., et al. 2011, A&A, 527, A18

Pereira, C. B., & Junqueira, S. 2003, A&A, 402, 1061

Persson, S. E., Cohen, J. G., Matthews, K., Frogel, J. A., & Aaronson, M. 1980, ApJ, 235, 452

Platais, I., Wyse, R. F. G., Hebb, L., Lee, Y.-W., & Rey, S.-C. 2003, ApJ, 591, L127

Ramírez, I., & Meléndez, J. 2005, ApJ, 626, 465

Royal Greenwich & Cape Observatories. 1966, Royal Observatory Annals, 2, I

Skrutskie, M. F., Cutri, R. M., Stiening, R., et al. 2006, AJ, 131, 1163

Smith, V. V., Suntzeff, N. B., Cunha, K., et al. 2000, AJ, 119, 1239

Sneden, C., & Parthasarathy, M. 1983, ApJ, 267, 757

Sneden, C., & Pilachowski, C. A. 1985, ApJ, 288, L55

Sollima, A., Pancino, E., Ferraro, F. R., & Bellazzini, M. 2006, Chemical Abundances and Mixing in Stars in the Milky Way and its Satellites, 156

Sollima, A., Pancino, E., Ferraro, F. R., et al. 2005, ApJ, 634, 332

Stancliffe, R. J., & Jeffery, C. S. 2007, MNRAS, 375, 1280

Stanford, L. M., Da Costa, G. S., & Norris, J. E. 2010, ApJ, 714, 1001

Stanford, L. M., Da Costa, G. S., Norris, J. E., & Cannon, R. D. 2006, ApJ, 647, 1075

Truran, J. W. 1981, A&A, 97, 391

van de Ven, G., van den Bosch, R. C. E., Verolme, E. K., & de Zeeuw, P. T. 2006, A&A, 445, 513

van Leeuwen, F., Le Poole, R. S., Reijns, R. A., Freeman, K. C., & de Zeeuw, P. T. 2000, A&A, 360, 472

Vanture, A. D. 1993, PASP, 105, 445

Vanture, A. D. 1992, AJ, 104, 1997

Vanture, A. D., Wallerstein, G., & Suntzeff, N. B. 2002, ApJ, 569, 984

Wallerstein, G., Iben, I., Jr., Parker, P., et al. 1997, Reviews of Modern Physics, 69, 995

Wood, P. R. 1985, Cool Stars with Excesses of Heavy Elements, 114, 357

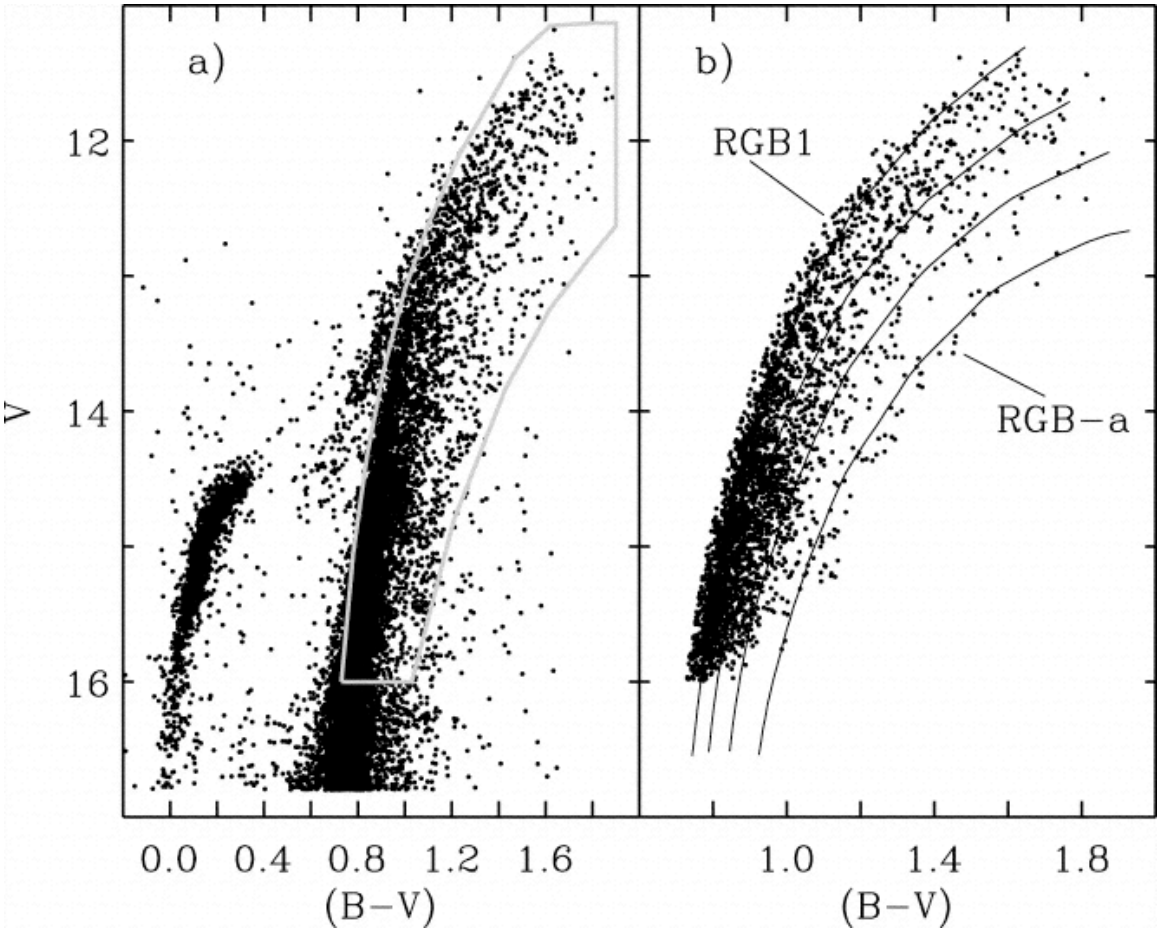

Fig. 1.— A color-magnitude diagram for giant members ω Cen , showing the obvious spread in and splitting of the red giant branch in the cluster. The appearance of the red giant branch and the main sequence in CMDs like this one constitute some of the evidence for multiple stellar generations in ω Cen. This figure is from Platais et al. (2003).

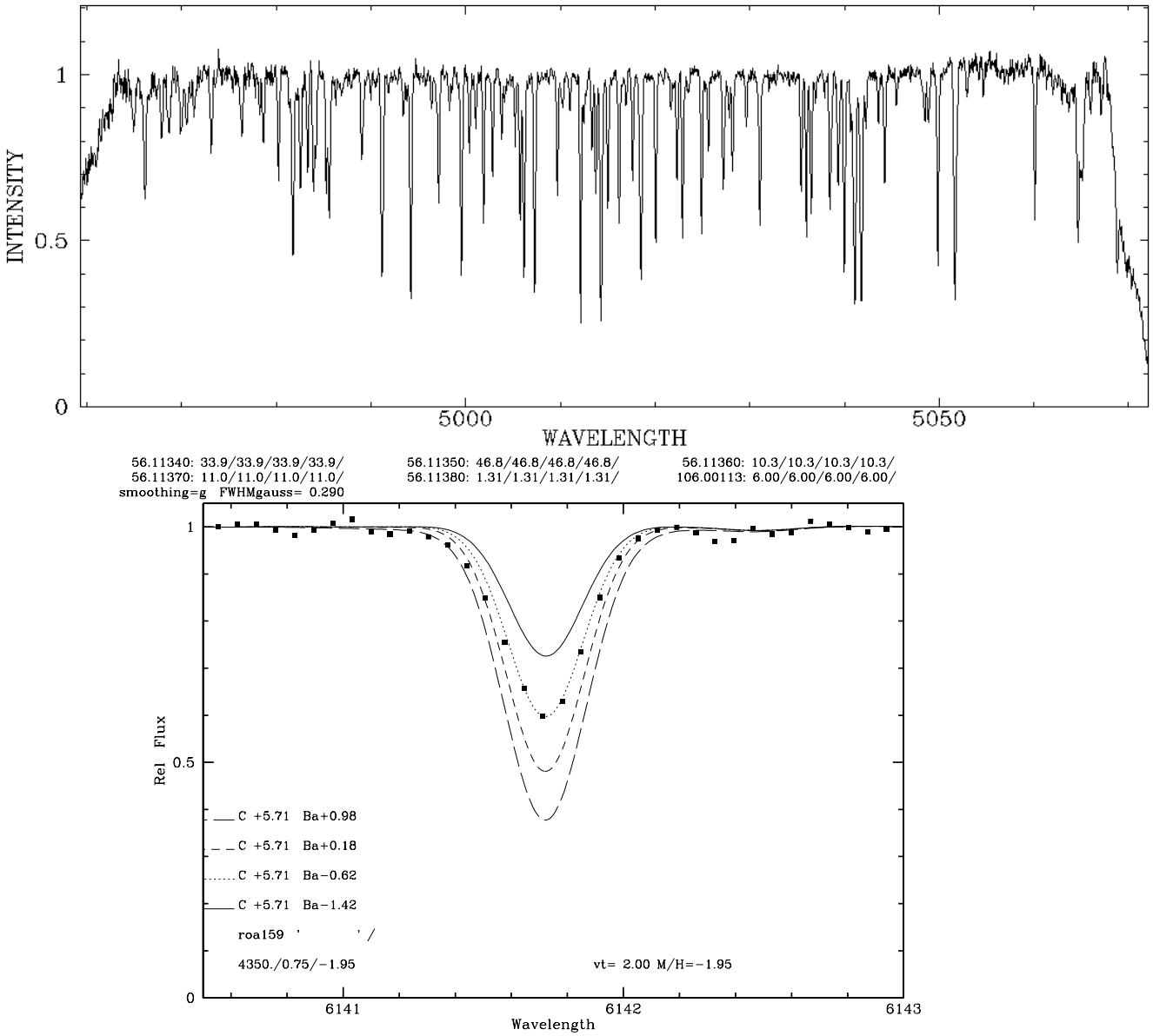

Fig. 2.— Examples of the spectroscopic data used in abundance analysis, both from ROA 159, a cluster giant. The top figure shows a roughly 100 $\mathring{A}$ span of the spectrum (one echelle order). The second figure shows a synthesis of the Ba-II spectral line at 6141 $\mathring{A}$. The figures were created using SPECTRE and MOOG.

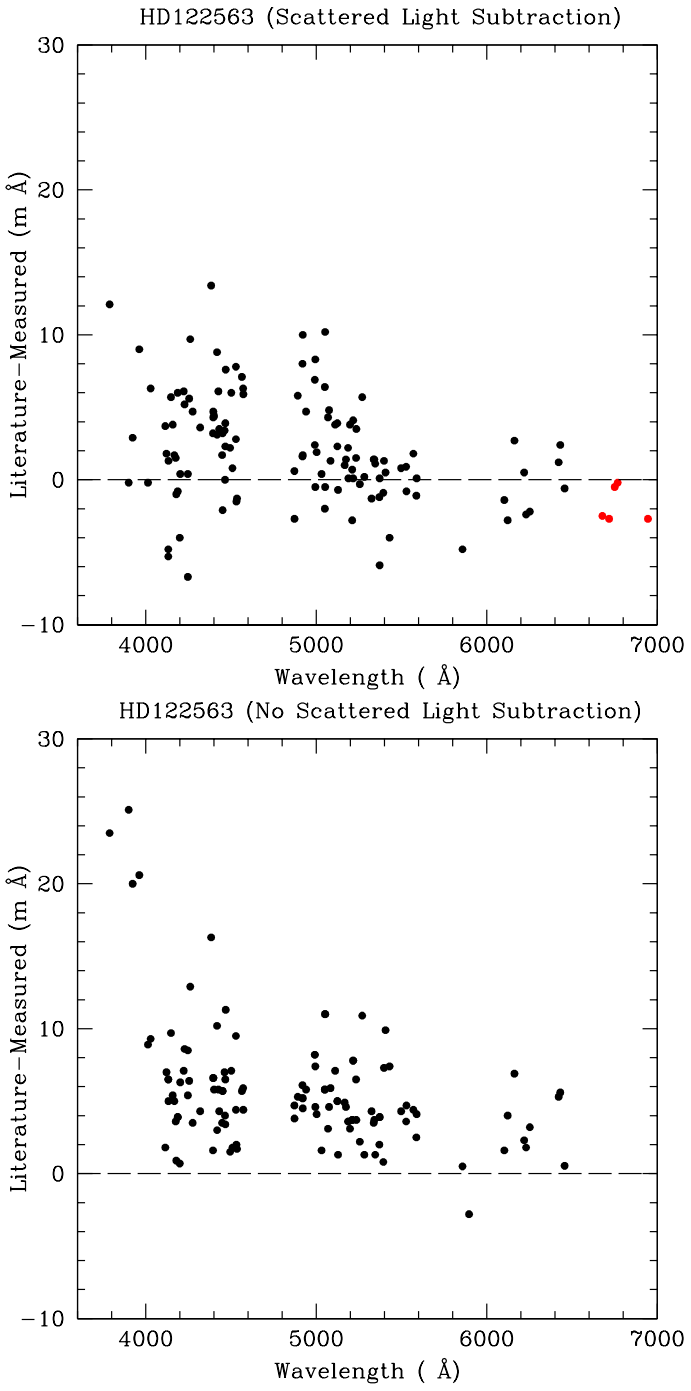

Fig. 3.— Comparison of measured equivalent widths to literature values from Cayrel et al. (2004), in black, and Johnson (2002), in red, for HD122563. The figure at left shows the deviation between measured and literature values when a scattered light subtraction is included, while the measurements in the right figure were made with no scattered light subtraction. There is a clear tendency to underestimate equivalent widths without the scattered light subtraction.

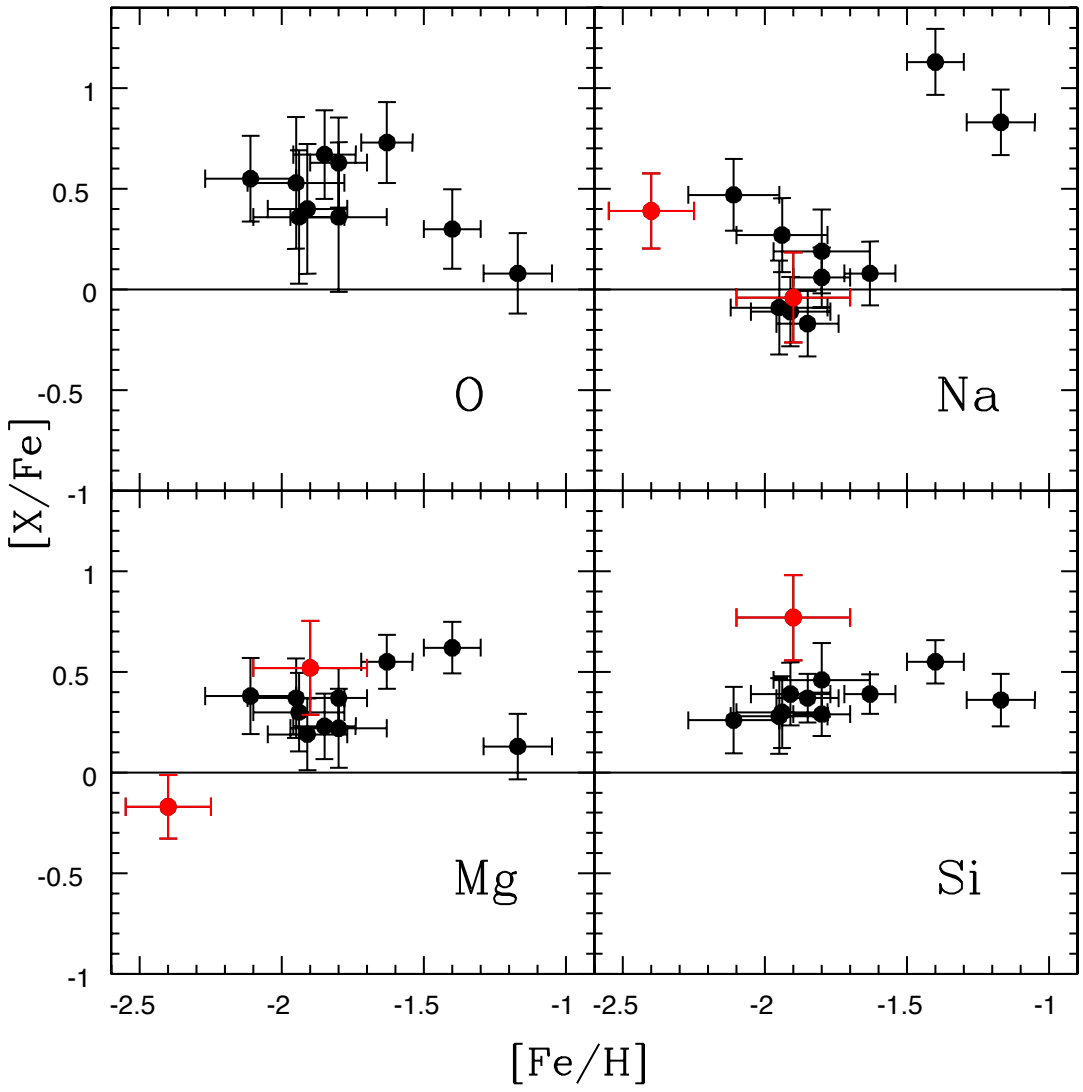

Fig. 4.— Abundances of O, Na, Mg, and Si relative to Fe as a function of metallicity. Red points indicate CH star abundances, while the black points correspond to red giants in ω Cen. It was not possible to measure oxygen abundances for the CH stars because the molecular bands make detecting the necessary line difficult. Oxygen-sodium anticorrelation?

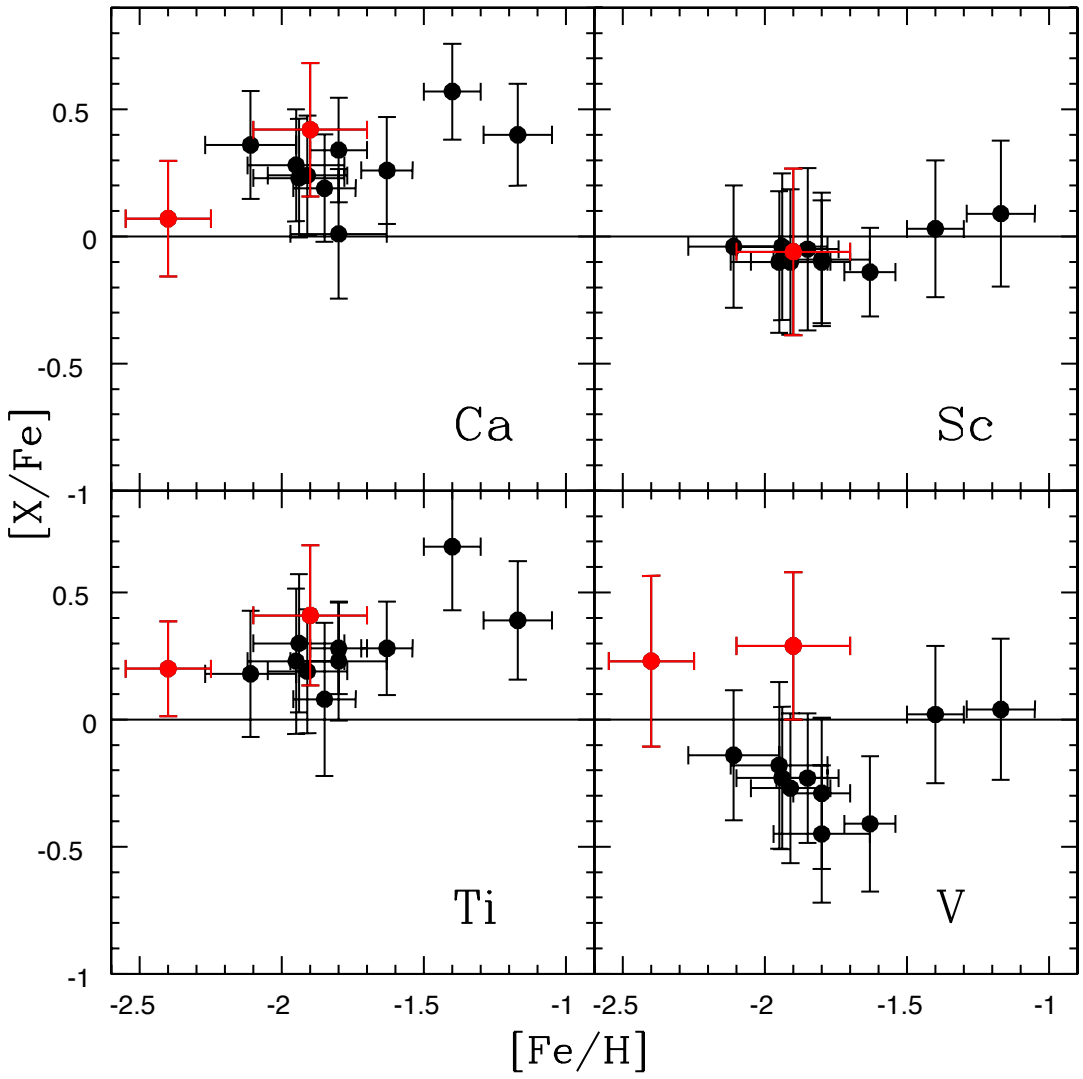

Fig. 5.— Abundances of Ca, Sc, Ti, and V relative to Fe as a function of metallicity. CH stars are again shown in red, while cluster red giant abundances are in black. Note that for most of these elements, the CH stars fit into general cluster trends in abundance as a function of metallicity.

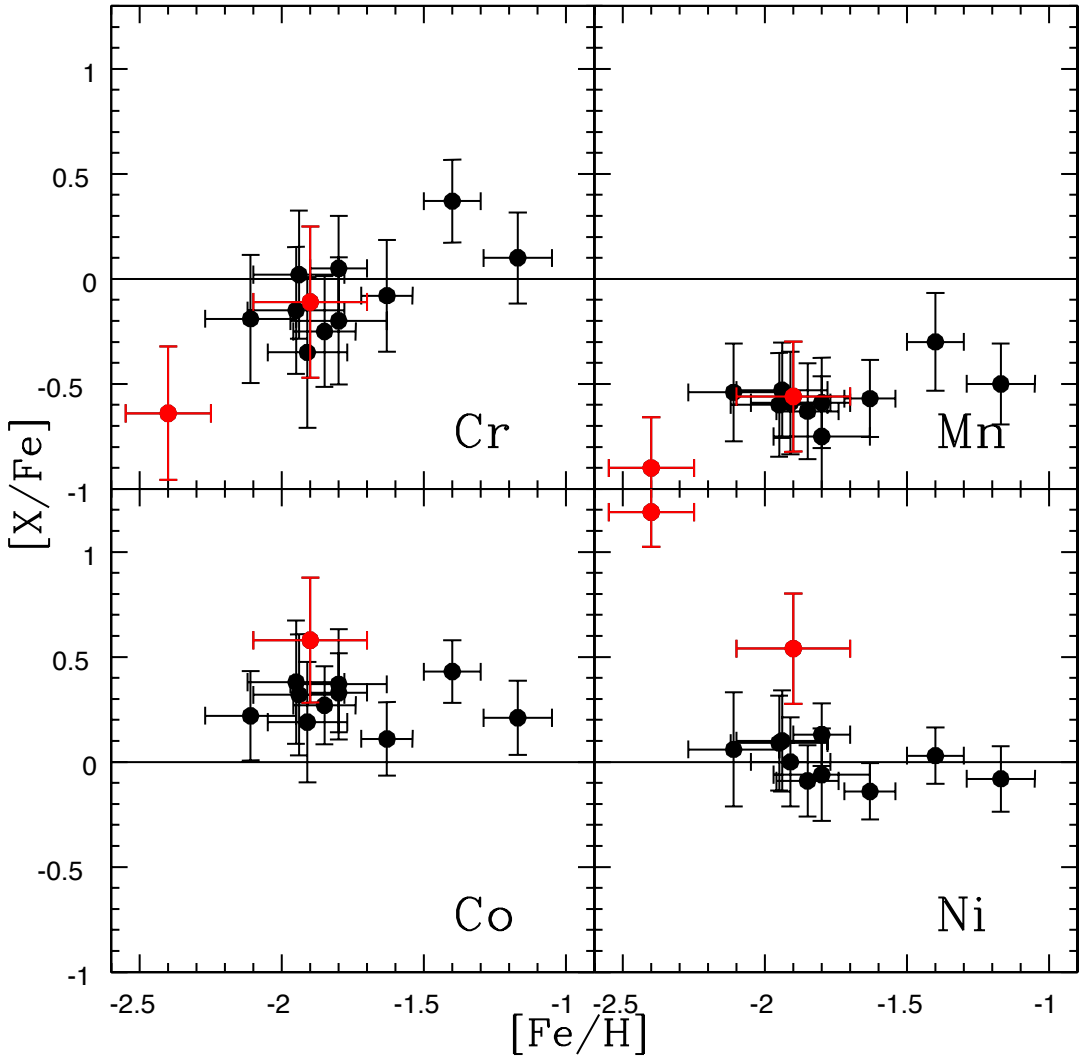

Fig. 6.— Abundances for the iron peak elements, including Cr, Mn, Co, and Ni, as a function of metallicity. Again, CH star abundances are in red, while those from cluster giants are in black. Eliminate that one Ni point?

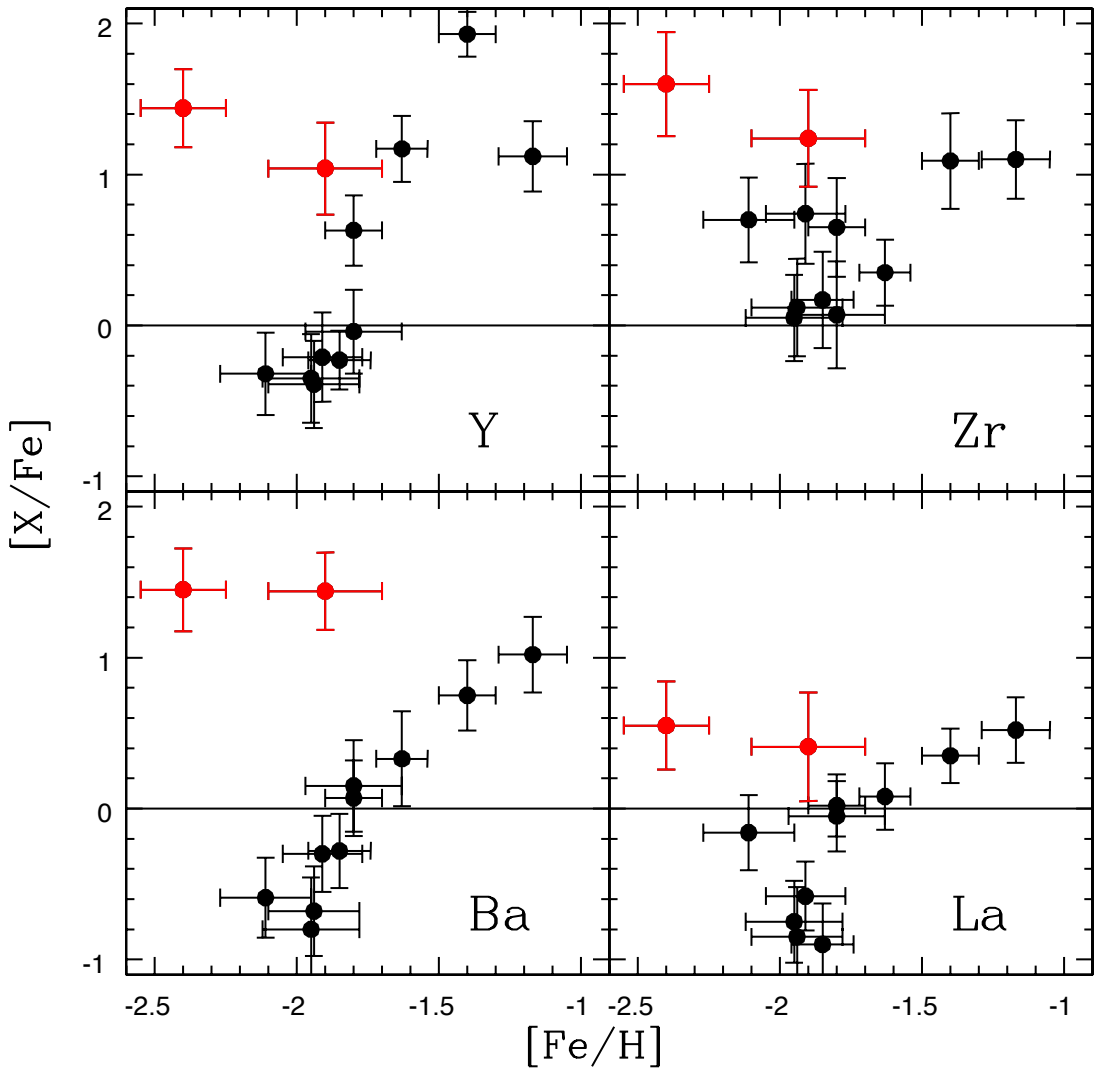

Fig. 7.— Abundances for the principal s-process elements, including Y, Zr, Ba, and La. The CH stars (in red) stand out as having dramatic enhancements in s-process abundances relative to cluster giants (in black) at the same metallicity. The chemical enrichment of ω Cen is also obvious, since s-process abundances increase (by approximately 2 dex) as a function of metallicity in the cluster giants.

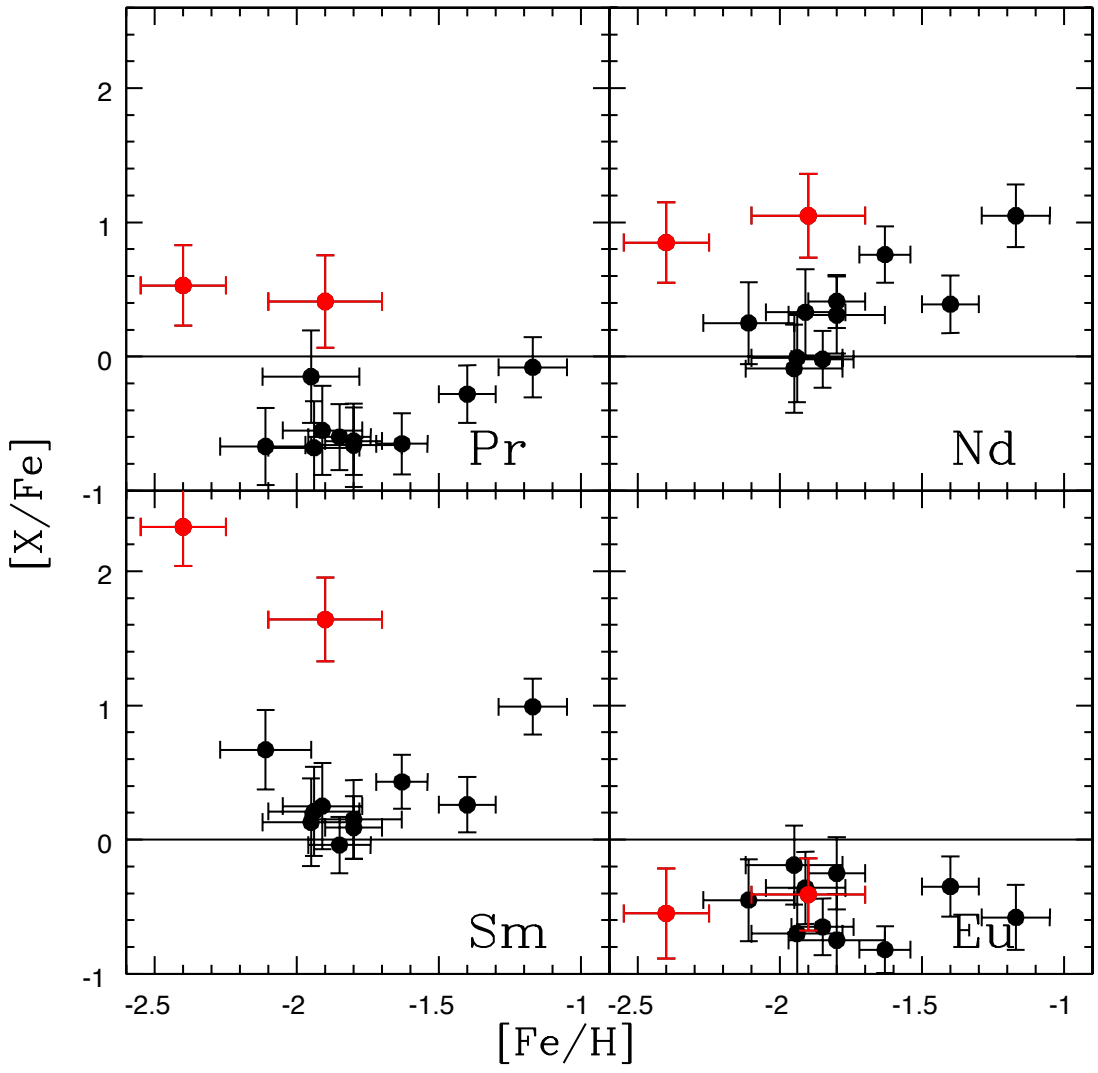

Fig. 8.— Abundances for Pr, Nd, Sm, and Eu for the CH stars (in red) and cluster giants (in black). We use Eu as the primary indicator of r-process enrichment. Unlike the s-process elements, the CH stars have roughly similar Eu abundances to other cluster giants at the same metallicity.

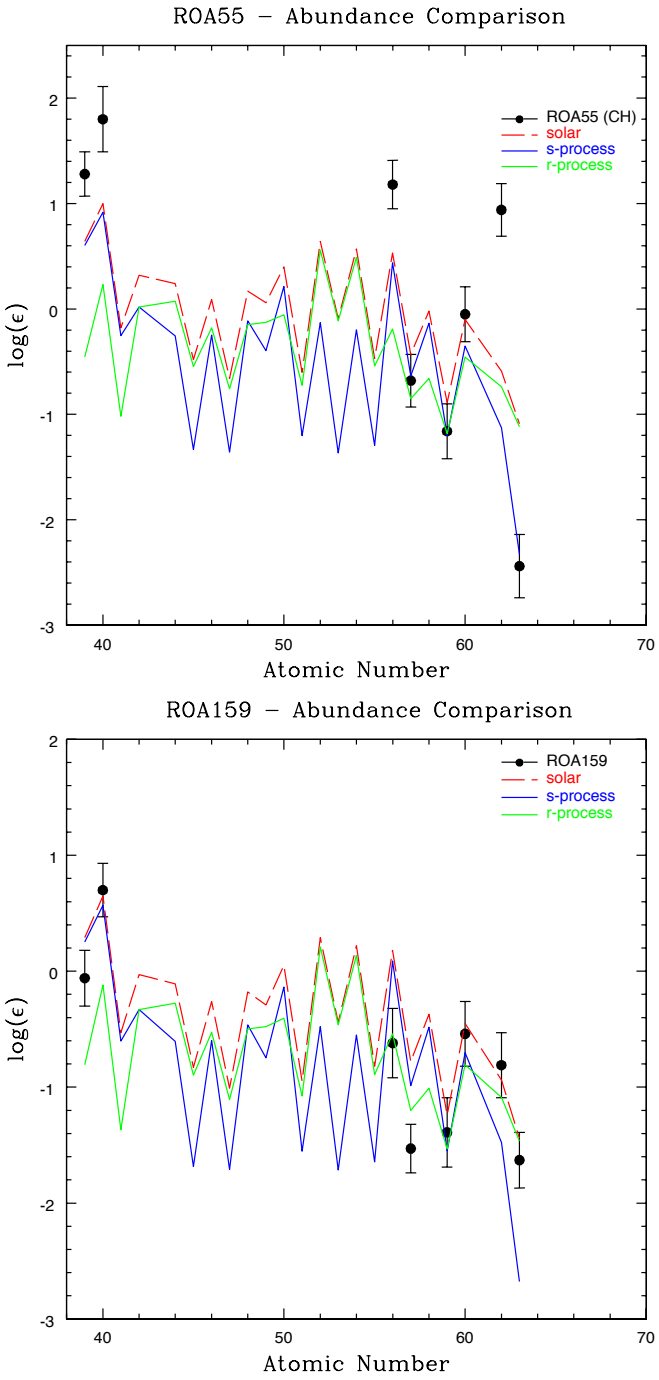

Fig. 9.— The neutron capture abundances of ROA 55 (a CH star) and ROA 159 are compared to the solar abundances and the theoretical yields of the r-process and s-process (cite!).

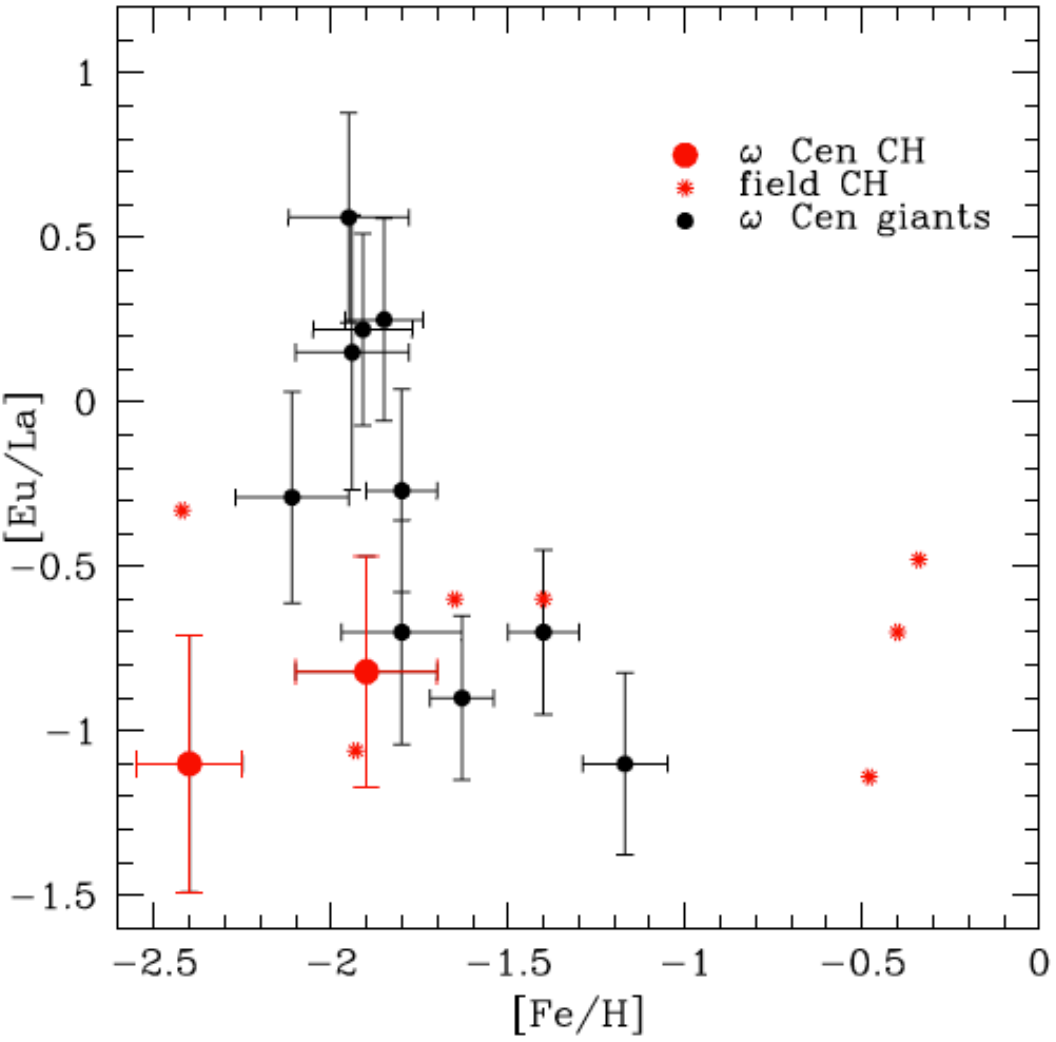

Fig. 10.— A comparison of the [La/Eu] ratio for ω Cen giants (in black) and CH stars (in red, solid points) to CH stars in the field (in red, stars). The [La/Eu] ratio probes the relative importance of the r-process and the s-process. Note that CH stars in ω Cen have similar [La/Eu] ratios to stars in the rest of the Galaxy.

Table 1. Target Stars

ROA	LEID	Obs. Date	RA (J2000) (h m s)	DEC (J2000) (deg m s)	V (mag)	K_s (mag)
40	46024	03/16/00	13 25 52.01	-47 30 16.3	11.291	7.954
43	10012	03/16/00	13 25 39.50	-47 14 05.4	11.529	7.706
46	25062	06/17/00	13 26 56.74	-47 20 52.6	11.583	7.839
52	48060	03/17/00	13 26 16.16	-47 30 56.1	11.316	7.763
55	52030	03/15/00	13 26 01.60	-47 33 05.8	11.431	7.645
56	24013	03/14/00	13 25 08.25	-47 20 19.6	11.596	7.801
58	25068	03/14/00	13 27 09.61	-47 20 51.4	11.542	8.176
61	26025	03/14/00	13 26 14.57	-47 21 22.8	11.411	7.757
66	52017	03/14/00	13 25 37.03	-47 33 00.4	11.435	7.730
67	35066	03/18/00	13 26 12.18	-47 25 30.4	11.444	8.000
70†	···	03/17/00	13 28 38.84	-47 26 32.6	11.580	7.834
73	40472	05/09/01	13 27 39.99	-47 27 31.3	11.463	7.748
76	48049	05/10/01	13 26 10.71	-47 31 20.2	11.525	7.912
85	47399	03/15/00	13 27 18.66	-47 30 50.9	11.701	7.957
96	23068	03/14/00	13 27 54.71	-47 19 32.1	11.658	8.191
108	50259	05/10/01	13 27 08.45	-47 31 49.2	11.714	7.859
109	69012	05/10/01	13 26 01.75	-47 40 33.5	11.666	8.414
110	57054	06/17/00	13 26 37.37	-47 35 04.7	11.589	7.989
158	61085	06/20/00	13 27 10.56	-47 37 00.2	11.846	8.081
159	33011	03/15/00	13 25 17.53	-47 24 26.5	11.879	8.715
162†	···	03/16/00	13 28 17.28	-47 34 10.7	11.990	8.251
166	52111	03/17/00	13 26 41.01	-47 32 49.7	12.437	8.329
171	51021	03/15/00	13 25 45.16	-47 32 38.2	11.984	8.424
172	21032	03/16/00	13 26 34.08	-47 19 00.4	11.947	8.620
179	41476	03/14/00	13 27 23.57	-47 28 07.1	12.031	7.960
199	67063	06/21/00	13 27 44.06	-47 39 29.8	12.084	8.873
200	31079	03/16/00	13 26 35.65	-47 23 31.1	12.151	9.211
201	39105	03/16/00	13 26 25.00	-47 27 06.3	12.262	7.822
219†	···	06/20/00	13 28 13.51	-47 24 23.2	12.160	8.413
229	34207	06/20/00	13 27 23.91	-47 24 34.4	12.221	9.011
240	6017	06/20/00	13 26 38.95	-47 12 16.3	12.333	8.808
243	34029	06/20/00	13 26 04.38	-47 25 00.8	12.107	8.719
245	15026	05/10/01	13 27 16.47	-47 15 58.4	12.234	9.004
255	61070	03/17/00	13 26 51.83	-47 36 48.1	12.161	9.224
266	54132	05/09/01	13 27 00.35	-47 33 53.4	12.275	9.300
267	46073	05/09/01	13 26 21.67	-47 30 20.1	12.544	9.182
270	55028	03/15/00	13 26 00.42	-47 34 30.8	12.247	8.821

Table 1—Continued

ROA	LEID	Obs. Date	RA (J2000) (h m s)	DEC (J2000) (deg m s)	V (mag)	K_s (mag)
279†	···	05/09/01	13 28 21.33	-47 20 29.7	12.320	9.182
292	31094	03/15/00	13 26 43.53	-47 23 19.9	12.405	9.570
300	48099	03/14/00	13 26 29.25	-47 31 09.3	12.443	8.444
316	76038	05/10/01	13 27 23.06	-47 43 55.4	12.535	9.049
320	42044	06/21/00	13 26 05.37	-47 28 20.6	12.321	7.757
322†	···	06/21/00	13 27 43.40	-47 32 18.0	12.450	···
334	39034	03/18/00	13 25 44.14	-47 27 12.3	12.513	9.535
362	21035	03/18/00	13 26 37.15	-47 19 00.5	12.457	9.547
367	55142	06/21/00	13 27 13.88	-47 34 17.8	12.442	9.086
378	56024	03/18/00	13 25 42.42	-47 34 53.1	12.717	9.539
418	55165	03/15/00	13 27 47.53	-47 34 06.5	12.649	9.775
429	49096	03/18/00	13 26 29.32	-47 31 35.6	12.813	10.095
447	37024	03/18/00	13 25 46.34	-47 25 59.5	12.719	8.471
474	32014	03/17/00	13 25 34.82	-47 23 47.7	12.809	10.048
476†	···	03/17/00	13 28 32.04	-47 34 17.1	12.770	9.939
500	48323	03/14/00	13 27 05.66	-47 31 04.8	13.081	9.273
513	35094	03/17/00	13 26 28.82	-47 25 23.4	12.897	8.558
517	34180	06/21/00	13 27 05.47	-47 24 37.0	13.030	9.239
538	42438	03/18/00	13 27 09.66	-47 28 27.8	13.067	10.020
548	5009	03/16/00	13 26 17.58	-47 11 30.9	12.912	10.040

Note. — Coordinates, identifiers and magnitudes for stars in the ω Cen sample. Most coordinates and V magnitudes are from the van Leeuwen et al. (2000) survey. †Coordinates and V magnitudes for these objects are from the Royal Greenwich and Cape Observatories (1966) survey. All K_s magnitudes are from the 2MASS Catalogue (Skrutskie et al. 2006).

Table 2. Stellar Parameters

ROA	T_{eff} spectroscopic (K)	T_{eff} color (K)	log(g) spectroscopic (cgs)	log(g) physical (cgs)	v_t spectroscopic (km/s)	[Fe/H] spectroscopic (dex)
40	4270	4210±37	0.50	0.58±0.06	2.10	-1.91
43	3900	3947±30	0.50	0.44±0.06	2.10	-1.85
46	4100	3986±30	0.50	0.50±0.06	2.00	-1.85
55	3900	3965±32	0.90	0.41±0.06	3.00	-2.40
58	4300	4192±39	0.60	0.66±0.06	2.00	-1.94
70	4250	3983±30	0.90	0.49±0.06	2.40	-1.90
159	4350	4320±41	0.75	0.89±0.06	2.00	-1.95
171	4050	4082±33	0.70	0.75±0.06	1.95	-1.80
219	3900	3983±29	0.55	0.73±0.06	1.95	-1.63
279	4450	4338±42	1.10	1.08±0.06	1.85	-1.83
362	4450	4505±48	0.80	1.25±0.06	1.75	-2.11
367	4350	4198±37	1.45	1.03±0.06	2.00	-1.17
500	3950	3954±29	1.15	1.06±0.06	1.80	-1.37
517	4050	4006±32	1.05	1.10±0.06	2.00	-1.40

Note. — Stellar parameters and associated uncertainties for some stars in the ω Cen sample. The typical uncertainty in the spectroscopic T_{eff} is 70 K, while the typical uncertainty in the spectroscopic $log(g)$ value is 0.2 dex. Uncertainties in the physical gravity and color-based effective temperature were determined by error propagation, while the uncertainties in v_t and [Fe/H] were determined according to the method in the text.

Table 3. Light Element Abundances

ROA	[Fe/H]	[O/Fe]	[Na/Fe]	[Mg/Fe]	[Si/Fe]	[Ca/Fe]	[Sc/Fe]	[Ti/Fe]
40	-1.91	0.40	-0.11	0.19	0.39	0.24	-0.10	0.19
43	-1.80	0.36	0.19	0.22	0.46	0.01	-0.09	0.23
46	-1.85	0.67	-0.17	0.23	0.37	0.19	-0.05	0.08
55	-2.40	···	0.39	-0.17	···	0.07	···	0.20
58	-1.94	0.36	0.27	0.30	0.30	0.23	-0.04	0.30
70	-1.90	···	-0.04	0.52	0.77	0.42	-0.06	0.41
159	-1.95	0.53	-0.09	0.37	0.28	0.28	-0.10	0.23
171	-1.80	0.63	0.06	0.37	0.29	0.34	-0.10	0.28
219	-1.63	0.73	0.08	0.55	0.39	0.26	-0.14	0.28
362	-2.11	0.55	0.47	0.38	0.26	0.36	-0.04	0.18
367	-1.17	0.08	0.83	0.13	0.36	0.40	0.09	0.39
500	-1.40	0.30	1.13	0.62	0.55	0.57	0.03	0.68

Note. — Abundances of light and α elements in the ω Cen sample. The metallicity ([Fe/H]) for each star is included, but all other element abundances are presented as a ratio compared to iron.

Table 4. Iron Peak Abundances

ROA	[Fe/H]	[V/Fe]	[Cr/Fe]	[Mn/Fe]	[Co/Fe]	[Ni/Fe]
40	-1.91	-0.27	-0.35	-0.59	0.19	0.00
43	-1.80	-0.45	-0.20	-0.75	0.37	-0.06
46	-1.85	-0.23	-0.25	-0.63	0.27	-0.09
55	-2.40	0.23	-0.64	-0.90	···	1.19
58	-1.94	-0.23	0.02	-0.53	0.32	0.10
70	-1.90	0.29	-0.11	-0.56	0.58	0.54
159	-1.95	-0.18	-0.15	-0.60	0.38	0.09
171	-1.80	-0.29	0.05	-0.59	0.33	0.13
219	-1.63	-0.41	-0.08	-0.57	0.11	-0.14
362	-2.11	-0.14	-0.19	-0.54	0.22	0.06
367	-1.17	0.04	0.10	-0.50	0.21	-0.08
500	-1.40	0.02	0.37	-0.30	0.43	0.03

Note. — Abundances of iron peak elements in the ω Cen sample. The metallicity ([Fe/H]) for each star is included, but all other element abundances are presented as a ratio compared to iron.

Table 5. Neutron Capture Element Abundances

ROA	[Fe/H]	[Y/Fe]	[Zr/Fe]	[Ba/Fe]	[La/Fe]	[Pr/Fe]	[Nd/Fe]	[Sm/Fe]	[Eu/Fe]
40	-1.91	-0.21	0.74	-0.30	-0.58	-0.55	0.33	0.25	-0.36
43	-1.80	-0.04	0.07	0.15	-0.05	-0.66	0.31	0.15	-0.75
46	-1.85	-0.23	0.17	-0.28	-0.90	-0.60	-0.02	-0.04	-0.65
55	-2.40	1.44	1.60	1.45	0.55	0.53	0.85	2.33	-0.55
58	-1.94	-0.39	0.12	-0.68	-0.85	-0.68	-0.01	0.21	-0.70
70	-1.90	1.04	1.24	1.44	0.41	0.41	1.05	1.64	-0.41
159	-1.95	-0.35	0.05	-0.80	-0.75	-0.15	-0.09	0.13	-0.19
171	-1.80	0.63	0.65	0.07	0.02	-0.63	0.41	0.09	-0.25
219	-1.63	1.17	0.35	0.33	0.08	-0.65	0.76	0.43	-0.82
362	-2.11	-0.32	0.70	-0.59	-0.16	-0.67	0.25	0.67	-0.45
367	-1.17	1.12	1.10	1.02	0.52	-0.08	1.05	0.99	-0.58
500	-1.40	1.93	1.09	0.75	0.35	-0.28	0.39	0.26	-0.35

Note. — Abundances of s-process and r-process elements in the ω Cen sample. The metallicity ([Fe/H]) for each star is included, but all other element abundances are presented as a ratio compared to iron.